ACS OMEGA

Open Access

http://pubs.acs.org/journal/acsodf

Article

Friendly Environmental Strategies to Recycle Zinc−Carbon Batteries for Excellent Gel Polymer Electrolyte (PVA-$ZnSO_4$-H_2SO_4) and Carbon Materials for Symmetrical Solid-State Supercapacitors

Thuy Trang T. Vuong, Huy-Trinh Phan, Nga Vu Thi Thu, Phi Long Nguyen, Huy Tiep Nguyen, Hoang V. Le, Nghia Trong Nguyen,* Thi Viet Bac Phung,* and Phuoc-Anh Le

Cite This: *ACS Omega* 2024, 9, 27710−27721

Read Online

ACCESS | Metrics & More | Article Recommendations | Supporting Information

ABSTRACT: In this report, we introduce a novel idea to prepare a redox additive in a gel polymer electrolyte system of PVA-$ZnSO_4$-H_2SO_4 based on zinc−carbon battery recycling. Here, zinc cans from spent zinc−carbon batteries are dissolved completely in 1 M H_2SO_4 to obtain a redox additive in an aqueous electrolyte of $ZnSO_4$-H_2SO_4. Moreover, carbon nanoparticles and graphene nanosheets were synthesized from carbon rod and carbon powder from spent zinc−carbon batteries by only one step of washing and electrochemical exfoliation, respectively, which have good electrochemical capability. The three-electrode system using a $ZnSO_4$-H_2SO_4 electrolyte with carbon nanoparticles and graphene nanosheets as working electrodes shows high electrochemical adaptability, which points out its promising application in supercapacitor devices. Thus, the symmetrical solid-state supercapacitor devices based on the sandwich structure of graphene nanosheets/PVA-$ZnSO_4$-H_2SO_4/graphene nanosheets illustrated the highest energy density of 39.17 W h kg^{-1} at a power density of 1700 W kg^{-1}. While symmetrical devices based on carbon nanoparticles/PVA-$ZnSO_4$-H_2SO_4/carbon nanoparticles exhibited a maximum energy density of 35.65 W h kg^{-1} at a power density of 1700 W kg^{-1}. Moreover, these devices illustrate strong durability after 5000 cycles, with approximately 90.2% and 73.1% remaining, respectively. These results provide a promising strategy for almost completely recycling zinc−carbon batteries, one of the most popular dry batteries.

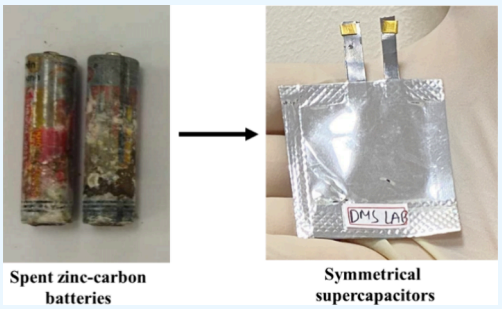

1. INTRODUCTION

Environmental pollution and its effects are the world's biggest problem facing humanity. Pollutants such as heavy metals, toxic gases, particulate matter, and macro-environmental pollutants pose a serious threat to human health.[1] Pollution control is a term used in environmental management. It includes the control of emissions and waste in air, water, and soil. Without pollution control, waste from consumption, production, transportation, the burning of heat-generating fuels, and other human activities will accumulate or release pollutants that will have many bad effects on the quality of the living environment.[2,3] Recycling waste is also a method to effectively reduce environmental pollution where the source of waste is large, causes a great deal of impact on the environment, and cannot be degraded, such as spent batteries.

Strategies to recycle spent batteries have become a very hot current research topic because of the rapid development of electronic technology and the electric vehicle market. Lithium-ion batteries have the most attraction due to their wide application in various electric vehicle types (electric cars, hybrid electric cars, electric bikes, etc.). However, there are various battery types, such as zinc−carbon, alkaline, and lead−acid, that have been used in electronic technology that require a complete recycling process. Among them, zinc−carbon batteries are an emergency candidate, which needs a suitable strategy for recycling because they are the most popular battery type on the market today. There are a hundred thousand tons of spent zinc−carbon batteries depleted every year, which raises a big question about the recycling strategy for this battery type.

Due to their excellent durability and higher energy density than traditional electrolytic capacitors and batteries, solid-state supercapacitors (SSCs) have been developed strongly with the contribution of various gel polymer electrolyte types. Here, the gel polymer electrolytes provide a strong electrostatic attraction between the charged groups and water molecules due to the presence of cations and anions, and it enhances the ion mobility in the electrolyte layer, enhancing ion diffusion performance.[4−6] Recently, Yan and co-workers reported the new polymer electrolyte C_3(Br)DMAEMA-PEGMA-HMPP-$LiSO_4$ with an activated carbon electrode for symmetrical SSCs, which

Received: April 24, 2024
Revised: May 29, 2024
Accepted: May 30, 2024
Published: June 13, 2024

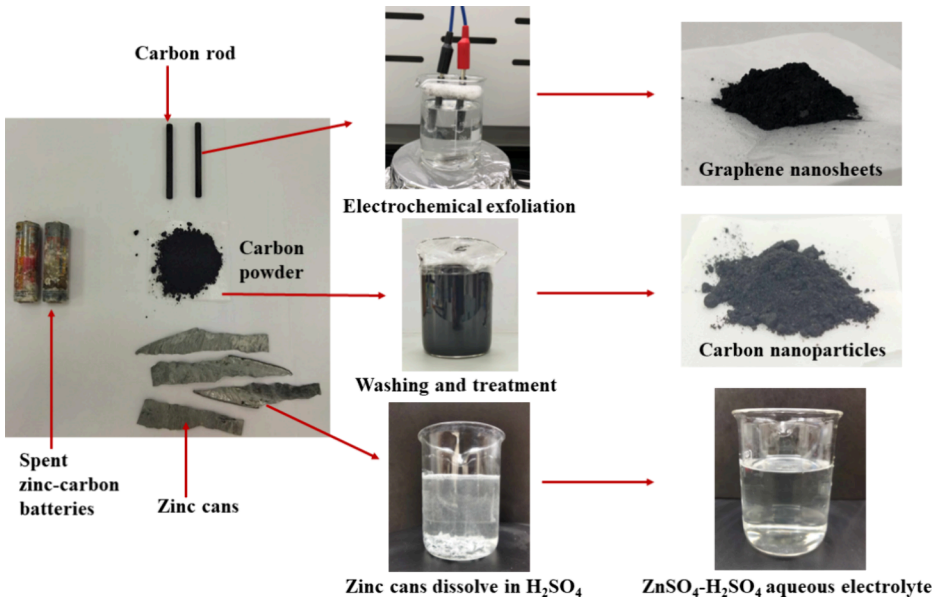

Figure 1. Process to prepare graphene nanosheets, carbon nanoparticles, and $ZnSO_4$-H_2SO_4 aqueous electrolyte.

delivered a specific capacitance of 64.92 F g^{-1} at 1 A g^{-1}.[4] In another study of gel polymer electrolyte for SSCs, Thanh et al. reported a couple of liquid ionized sodium salts with PVA to make the PVA-PEO-CH_3COONa-Na_2SO_4 system and graphene nanoplatelet electrodes that showed a maximum capacitance of 93.768 F g^{-1} at 1 A g^{-1}.[6] The polymer electrolyte [{PVdF(HFP)-EDiMIM(BF_4)}(7:3)] (20 wt %)-(PC-Mg-$(ClO_4)_2$(0.3M)] (80 wt %) with activated carbon electrode for symmetrical solid-state supercapacitors has achieved a capacitance of 868 mF cm^{-2} according to Gupta et al.[7] Guo and co-workers reported that a new cationic monomer, *N*-(2-methacryloyloxy)ethyl-*N*,*N*-dimethylpoly(ethylene glycol)-ammonium chloride ($(EO)_6$(Cl)DMAEMA), was created by using the alkylation process. This amorphous structure is made possible by its thermal copolymerization with poly(ethylene glycol) methacrylate (PEGMA), which creates a flexible polycation gel polymer electrolyte (PGPE) matrix. This PGPE was soaked in Li_2SO_4/H_2O with two symmetric activated carbon electrodes that made up a supercapacitor with a capacitance of 61.4 F g^{-1} at 1 A g^{-1}.[8] Chi et al. introduced the novel electrolyte PVDF-HFP/LiBOB, which was used for the GO/CNT/PSE electrode for a symmetrical supercapacitor that obtained a typical capacitance of 267 F g^{-1} at 1 A g^{-1}.[9] In a report by Yong et al., research on a new electrolyte called i_ANGPE has shown a maximum capacitance of 46.6 F g^{-1} at 0.13 A g^{-1} with two electrodes that are symmetric activated carbon and assembled in a glovebox filled with Ar.[10] To investigate a novel idea combining both a new redox additive and a recycling battery, we introduced solid-state supercapacitors with gel polymer electrolytes consisting of PVA as the polymer host frame and a $ZnSO_4$-H_2SO_4 mixture as an ionic liquid. It can be seen that the advantages of this electrolyte are low-cost, high ionic conductivity, easy synthesis at room temperature, and moreover, being able to take advantage of the zinc cans from spent zinc-carbon batteries. Based on previous research, in this study we present a new idea to synthesize an electrolyte system incorporating a redox additive in an aqueous electrolyte by utilizing the zinc cans in spent zinc–carbon batteries. Thus, our idea in this article is to completely recycle spent zinc–carbon batteries by recycling all the components that will minimize the effects of spent batteries being discharged into the environment.

In this report, we provide an interesting strategy to prepare the redox additive $ZnSO_4$ in the gel polymer electrolyte system based on PVA-H_2SO_4, which uses zinc cans from spent zinc–carbon batteries. In one step of completely dissolving zinc cans in a 1 M H_2SO_4 solution, the mixture electrolyte $ZnSO_4$-H_2SO_4 obtains a very high ionic conductivity of 183 mS cm^{-1} at 25 °C, and the gel polymer electrolyte (PVA-$ZnSO_4$-H_2SO_4) still reaches a high value of 81 mS cm^{-1} at 25 °C.

2. EXPERIMENTS

2.1. Materials. Spent zinc–carbon batteries were collected from a supermarket. Sulfuric acid (H_2SO_4, 95%) was purchased from Samchun, China. Poly(vinyl alcohol) (PVA, 99%) was ordered from Mackalin. *N*-Methylpyrrolidone (NMP), *N*,*N*-dimethyiformamide (DMF, AR), and polyvinylidene difluoride (PVDF) were ordered from Shanghai Zhanyun Chemical Co. Ltd., China. Carbon paper substrate was ordered from Homytech, Taiwan. Table salt was purchased at a supermarket. Commercial activated carbon was purchased from Dmregent.

2.2. Preparation of Carbon Nanoparticles and Graphene Nanosheets. Carbon nanoparticles were prepared by one simple step of washing before drying and grinding to obtain the final product (Figure 1), following our previous report.[11] First, 2 g of carbon waste from spent zinc–carbon batteries was collected and transferred into 200 mL of ethanol with ultrasonics for 6 h to clean the remaining binder remaining. Second, this mixture was filtrated, washed several times with DI water, and dried in a vacuum oven at 80 °C for 48 h to obtain carbon powder. Then, finally, this carbon powder was ground carefully in a ceramic cup to reach carbon nanoparticles, namely, C_{NPs}.

Graphene nanosheets were prepared by a simple electrochemical exfoliation process in kitchen table sea salt. Two carbon rods were collected from spent zinc–carbon batteries and used as two electrodes, which were immersed in kitchen table salt at 10% under a DC power supply of 3.5 V for 24 h (Figure 1). Then, the final solution was filtrated, washed several times with DI water and ethanol, and dried at 80 °C in a vacuum oven for 48 h to obtain graphene nanosheets, namely Gs.

https://doi.org/10.1021/acsomega.4c03948
ACS Omega 2024, 9, 27710−27721

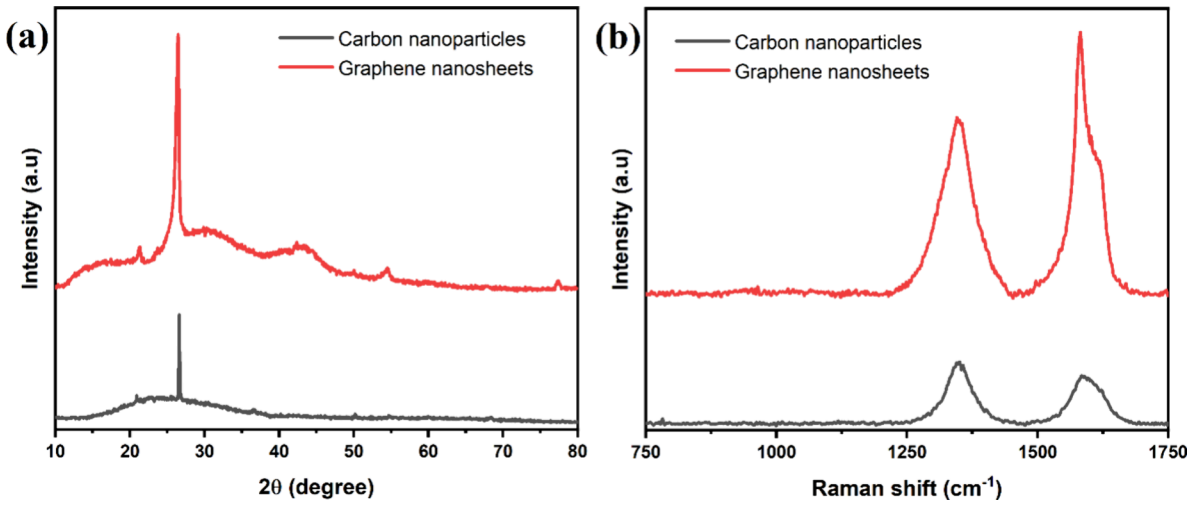

Figure 2. (a) XRD pattern and (b) Raman spectroscopy of C_{NPs} and Gs.

The structure and morphology of C_{NPs} and Gs are studied by following various techniques, including X-ray diffraction (XRD, Bruker D8 PHASER with a Cu Kα tube), Raman spectroscopy (Horiba Jobin Yvon laser source with an excitation wavelength of 532 nm), and scanning electron microscopy (SEM, JEOL, JSM-IT800).

2.3. Preparation of ($ZnSO_4$-H_2SO_4) Aqueous Electrolyte and (PVA-$ZnSO_4$-H_2SO_4) Gel Polymer Electrolyte. ($ZnSO_4$-H_2SO_4) aqueous electrolyte was prepared in one simple step. Here, 12.5 g of zinc cans from spent zinc−carbon batteries was dissolved completely in 200 mL of 1 M H_2SO_4 and kept stable for 3 days to completely dissolve the zinc cans (Figure 1 and Supporting Video 1) to obtain an aqueous electrolyte solution of $ZnSO_4$-H_2SO_4 used for three-electrode system studies. Gel polymer electrolyte was prepared by the solution mixing method: 100 mg of PVA was dissolved in 10 mL of $ZnSO_4$-H_2SO_4 with constant stirring at 100 °C for 2 h to obtain a homogeneous, clear gel solution. This gel polymer electrolyte was used for the fabrication of symmetrical solid-state supercapacitor devices. Here, the ionic conductivity of aqueous electrolyte and gel polymer electrolyte was studied by the Multiparameter Portable Meter PC 950, Apera instruments.

2.4. Electrochemical Studies. The carbon nanoparticles (C_{NPs}) and graphene nanosheet (Gs) electrodes were prepared by the solution coating method. First, 80 mg of active materials (C_{NPs} or Gs; 80 wt %), 10 mg of CNT (10 wt %), and 10 mg of PVDF (10 wt %) were mixed together in 3 mL of NMP with constant stirring at 80 °C and reduced to 27 °C for 3 days to obtain homogeneous slurries. Then, 30 μL of this slurry was coated on a carbon paper substrate over an area of 1.5 × 1.5 cm (2.25 cm^2) (Figure S1), then dried at 80 °C under a vacuum environment for 3 days to obtain working electrodes with 1 mg of each electrode.

The three-electrode system was setup with a graphene electrode as the working electrode, Pt foil as the counter electrode, Ag/AgCl as the reference electrode, and $ZnSO_4$-H_2SO_4 aqueous electrolyte.

The symmetrical solid-state supercapacitors were fabricated following the sandwich structure: active materials/PVA-$ZnSO_4$-H_2SO_4/active materials. Two electrodes were immersed in the PVA-$ZnSO_4$-H_2SO_4 gel polymer electrolyte. Then, one piece of 2 × 2 cm (4 cm^2) of oil absorbent paper was immersed in gel polymer electrolyte, and it was fabricated between two electrodes following the pouch cell type (Supporting Video 2).

The electrochemical studies of the supercapacitors were studied on an electrochemical workstation CS310 (Corrtest, China) by following various techniques including cyclic voltammetry (CV), electrochemical impedance spectroscopy (EIS), and galvanostatic charge−discharge (GCD). Here, the specific capacitance of the supercapacitor (C_{CV}, F g^{-1}) was calculated from CV, using the following equations:[11,12]

$$C_{CV} = \frac{\int I \, dV}{2 \times (V_2 - V_1) \times m \times v} \quad (1)$$

where I (A) is the applied current, $\Delta V = (V_2 - V_1)$ (V) is the working voltage window, m (g) is the total mass volume of electrode material, and v is the scan rate (V s^{-1}).

Moreover, the specific capacitance of the three-electrode system (C_{GCD}, F g^{-1}) and the symmetrical solid-state super capacitor (SSC) device (C_s, F g^{-1}) were calculated from the charge−discharge curve, using the following equations:[11,12]

$$C_{GCD} = \frac{I \times \Delta t}{\Delta V \times m} \quad (2)$$

$$C_s = 4C_{GCD} \quad (3)$$

The energy density (E, W h kg^{-1}) and power density (P, W kg^{-1}) were calculated by the following equations:[11,12]

$$E = \frac{C_i \times (\Delta V)^2}{2} \times \frac{1000}{3600} \quad (4)$$

$$P = \frac{E \times 3600}{\Delta t} \quad (5)$$

where C_i is the capacitance of working electrode in the three-electrode system (C_{GCD}) or specific capacitance of devices (C_s) and Δt (s) is the discharge time.

3. RESULTS AND DISCUSSION

3.1. Preparation of Graphene Nanosheets. In this report, graphene nanosheets were prepared by one step of electrochemical exfoliation, which focused on recycling zinc−carbon batteries (Figure 1). This method provides an excellent strategy to synthesize graphene materials from waste elements in

https://doi.org/10.1021/acsomega.4c03948
ACS Omega 2024, 9, 27710−27721

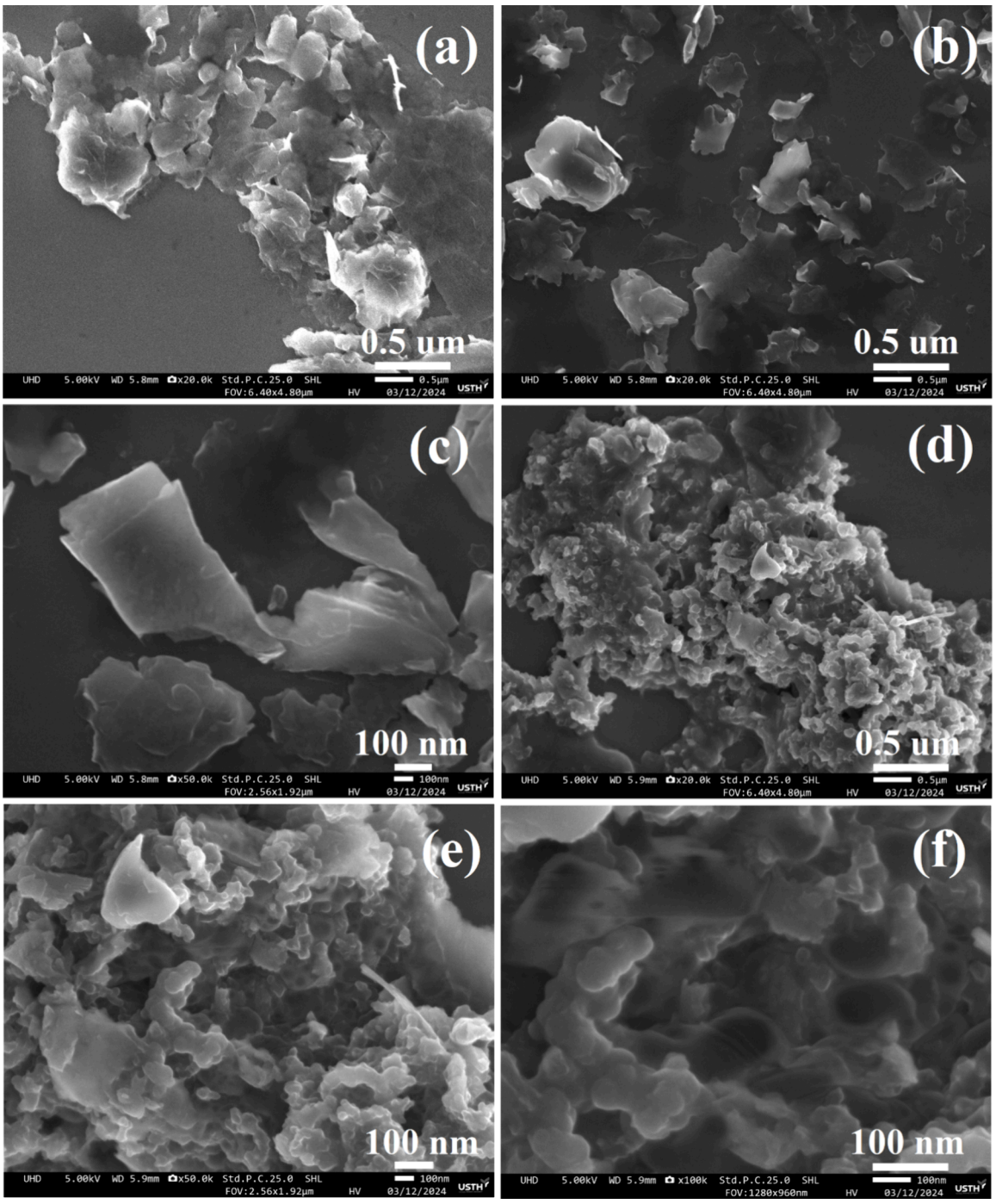

Figure 3. SEM images of Gs (a, b, c) and C_{NPs} (d, e, f) at various magnifications.

electronic waste, which is considered an invincible research trend.

The resulting morphological structures of Gs and C_{NPs} materials were determined and studied by XRD and Raman measurements (Figure 2). From the XRD pattern in Figure 2a, the C_{NPs} powder sample depicts mostly an amorphous phase but still has a weak crystal phase at $2\theta = 26.5°$, corresponding to (002) belonging to the graphite phase.[13−17] Here, the Gs powder sample shows a high crystalline property with strong broadening peaks at the position $2\theta = 26.5°$ relating to the carbon crystal lattice arranged parallel to make a graphene two-dimensional structure, which is consistent with the SEM measurement results in Figure 3.[15−17] Figure 2b shows the Raman spectra of C_{NPs} and Gs samples with clearly defined D and G bands. It can be observed that the D band with a peak located at position 1350.35 cm^{-1} represents the disordered structure of the material, and the G band located at position 1568.76 cm^{-1} represents the crystallinity of the graphite phase, which has shown that the structure of this material is consistent with the XRD measurement results.[14]

Figure 3 shows an SEM image of the C_{NPs} and G_S samples. Through the images with increasing bandwidth, it is clear that the characteristic wrinkles and folds of graphene nanosheets have been created and are a size of several micrometers (Figure 3a,b). Moreover, the contour of graphene can be clearly seen from Figure 3c, which is one of the typical features of graphene,

https://doi.org/10.1021/acsomega.4c03948
ACS Omega 2024, 9, 27710−27721

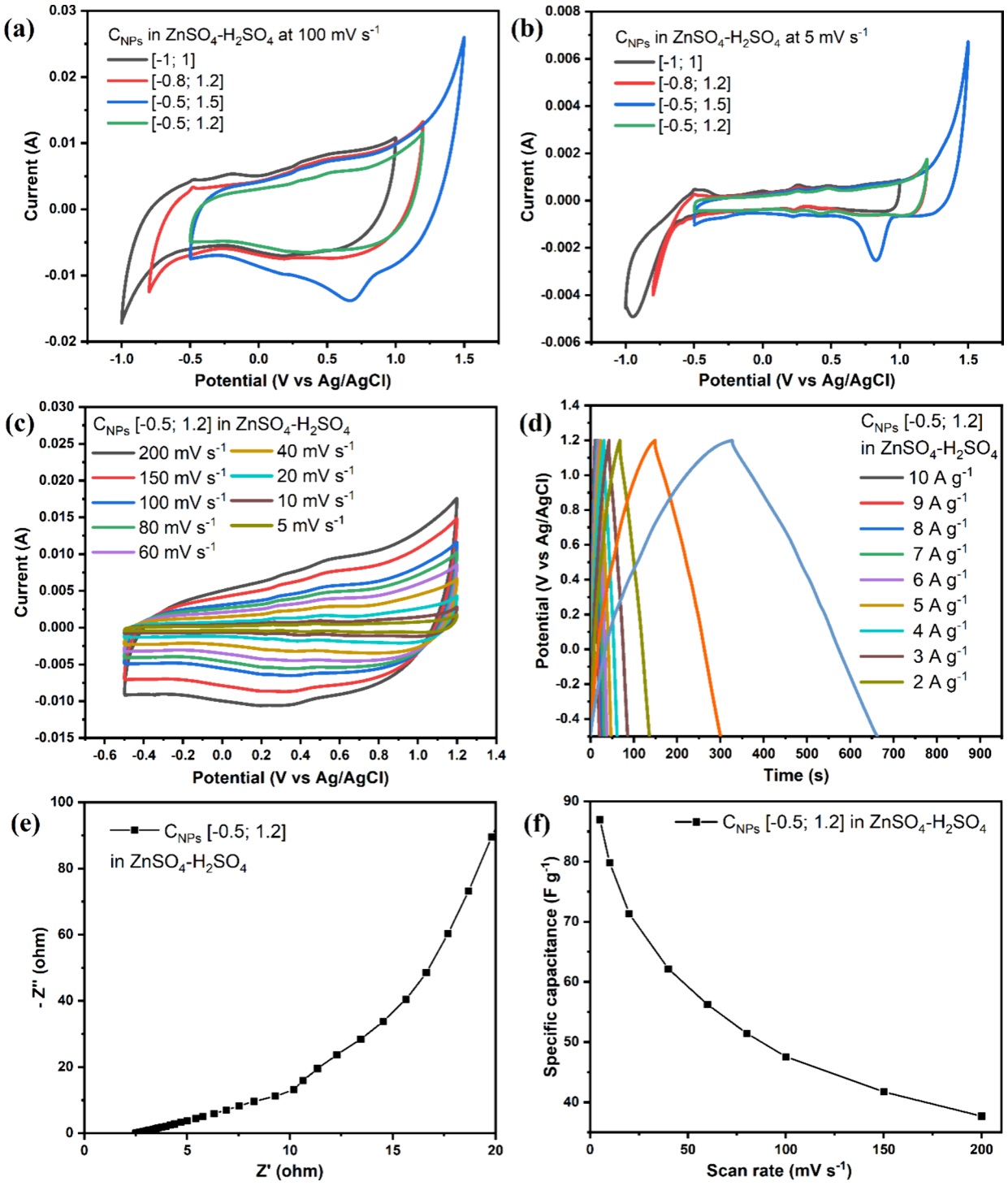

Figure 4. Electrochemical studies of the three-electrode system for C_{NPs}: CV curves at different working voltage windows at (a) 100 and (b) 5 mV s^{-1}, respectively, (c) CV curves, (d) GCD curves, (e) EIS plot, and (f) specific capacitance following scan rates.

and the small columnarity may be a dispersant. These results confirm that two-dimensional graphene nanosheets can be produced by the electrochemical exfoliation process in kitchen table salt. Figure 3d,e,f shows the small, unique particle sizes of carbon nanoparticles, which have a porous structure and spherical shapes with an average size of around 50 nm. This structure could enhance the solution dispersion of carbon nanoparticles, leading to a unique supercapacitor electrode layer.

3.2. Electrochemical Characterizations. *3.2.1. Electrochemical Studies of Three Electrode System.* Figure 4 indicates the electrochemical properties of C_{NPs} materials by measuring the three-electrode system in 1 M $ZnSO_4$-H_2SO_4 aqueous electrolyte. Here, these materials provide promising electrochemical capabilities for the double-layer capacitors. As current flows through the electrodes, ions will be separated and diffused into the opposite electrode (negative ions will move to the anode; positive ions will move to the cathode) and form two electrostatic layers on either side. To investigate the active

https://doi.org/10.1021/acsomega.4c03948
ACS Omega 2024, 9, 27710−27721

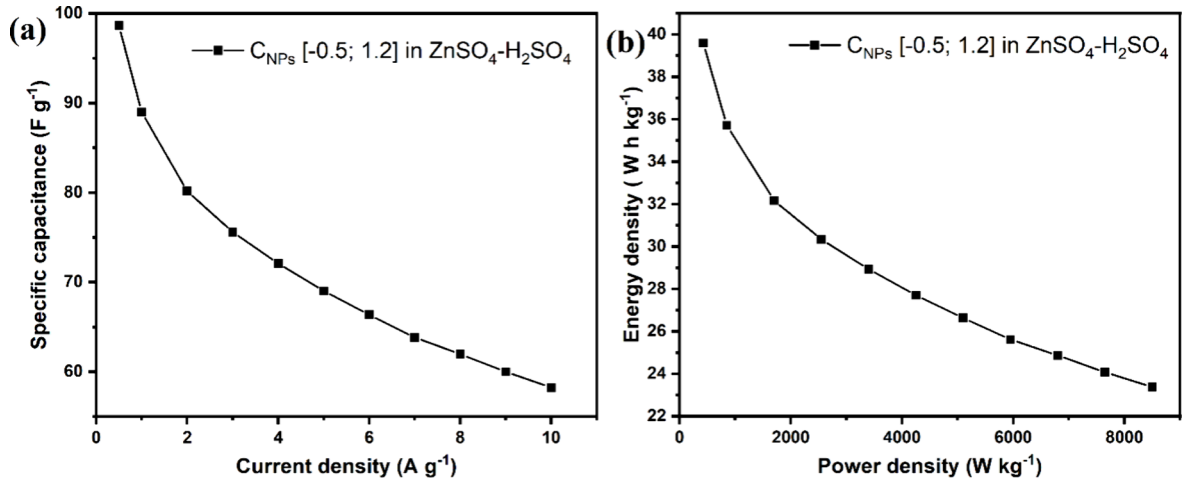

Figure 5. Electrochemical studies of the three-electrode system for C_{NPs}: (a) specific capacitances following current densities and (b) energy densities following power densities.

Table 1. Electrochemical Studies of Carbon Materials in This Report with Previous Data

Material	Method to preparation	Electrolyte	Specific capacitance	Energy density	Ref
CNT	CVD	KOH activation	53.6 F g^{-1} at 50 mA g^{-1}	N/A	33
Activated carbon	Spray coating	PVA/ADP	39.8 F g^{-1} at 0.12 mA cm^{-2}	205 μW h^2 cm^{-2}	34
Banana fiber-derived activated carbon	Pyrolysis	1 M Na_2SO_4	74 F g^{-1} at 0.5 A g^{-1}	N/A	35
Graphene nanosheets _ H^+	Plasma exfoliation	1 M NaCl	67.1 F g^{-1} at 5 mV s^{-1}	N/A	36
Graphene nanosheets _ Na^+			21.6 1 F g^{-1} at 5 mV s^{-1}		
Graphite			11.4 1 F g^{-1} at 5 mV s^{-1}		
Surface-exfoliated graphite pencil electrodes	Surface exfoliation	0.1 M H_2SO_4	53.6 mF cm^{-2} at 0.1 mA cm^{-2}	7.4 μW h cm^{-2}	37
Expanded graphite foil	Electrochemical expansion	1 M H_2SO_4	65 mF cm^{-2} at 20 mA cm^{-2}	N/A	38
Graphene nanosheets	Cathodic plasma exfoliation	1 M KOH	61 F g^{-1} at 0.5 A g^{-1}	12.125 W h kg^{-1}	39
Carbon nanoparticles	Treatment	1 M $ZnSO_4$·H_2SO_4	98.64 F g^{-1} at 0.5 A g^{-1}	39.59 W h kg^{-1}	This work
Gs	Electrochemical exfoliation	1 M $ZnSO_4$·H_2SO_4	149.68 F g^{-1} at 0.5 A g^{-1}	60.08 W h kg^{-1}	This work

region of the C_{NPs} in the new electrolyte, we conducted a survey of the active region of the material in four different working voltage windows. Figure 4a,b shows the results of a comparison of the CV curves of C_{NPs} at different scan rates at 100 and 5 mV, respectively. At 100 mV s^{-1}, different CV curves (Figure 4a) showed redox peaks in the investigated areas of [−1; +1], [−0.8; +1.2], and [−0.5; +1.5], and the peaks are stronger at a scan rate of 5 mV s^{-1} (Figure 4b), which shows the strong redox and reduction reactions of the redox additive electrolyte. Therefore, we chose the best stability region of the material as about [−0.5; +1.2] to further investigate the electrochemical properties. The CV diagram of C_{NPs} in a working voltage window of [−0.5; +1.2] at different scanning rates shows the stability and linearity of the $ZnSO_4$-H_2SO_4 system (Figure 4c). The CV curve decreases with a decrease in scanning speed from 200 mV to 5 mV, and they are shaped almost like a rectangle, which indicates that the electric double layer capacity closely resembles that of an ideal supercapacitor.[18−20] To investigate the discharge of C_{NPs} in the new electrolyte solution, we conducted a GCD measurement survey at different current densities from 10 to 0.5 A g^{-1} in the range [−0.5; +1.2], which are shown in Figure 4d. Here, GCD curves are shaped almost identical to triangles with high symmetry, which indicates that the conductivity of the material through the electrode is stable, has a high specific capacitance, reversibility, and excellent discharge properties.[21,22] Figure 4e depicts electrochemical impedance spectroscopy (EIS) measurements of C_{NPs} in the frequency range from 100 kHz to 100 mHz at open-circuit potentials with an AC amplitude of 5 mV. The EIS diagram shows that the linear slope of Nyquist cells in the low-frequency region confirms mass transfer, which indicates faster diffusion of ions in the electrolyte.[23,24] The relatively equivalent serial resistance of EIS measurements of supercapacitors illustrates the high ionic conductivity and good electrochemical capacitive ability.[25,26] The equivalent resistance of C_{NPs} has a value of around 2.5 Ω. Here, the equivalent series resistance includes the resistance of the electrode to the electrolyte, the intrinsic resistance of the electrode, and the resistance of electrolyte $ZnSO_4$-H_2SO_4. Based on the CV curve, the specific capacitance of the C_{NPs} working electrode has been specifically calculated at different scanning rates based on eq 1 shown in Figure 4f. The C_{NPs} electrode obtained the highest specific capacitance of 86.95 F^{-1} at a scan rate of 5 mV s^{-1}. As can be seen, the CV curves still show a linear increase with the increase in scanning rates, which proves the excellent ionic diffusion at the electrode/electrolyte interface during measurement.[27,28]

Moreover, the specific capacitance of the C_{NPs} object at different current densities was calculated through a GCD curve based on eqs 2, 4, and 5 and is shown in Figure 5a. At a high current density of 10 A g^{-1}, the C_{NPs} working electrode has a specific capacitance of 58.23 F g^{-1} and obtains the highest value of 98.64 F g^{-1} at 0.5 A g^{-1}. The results indicate a good electrochemical capability in comparison to other previous reports in Table 1. Figure 5b shows the relationship between the energy density and power density of C_{NPs} working electrodes through the Ragone plot that can be calculated from the GCD

https://doi.org/10.1021/acsomega.4c03948
ACS Omega 2024, 9, 27710−27721

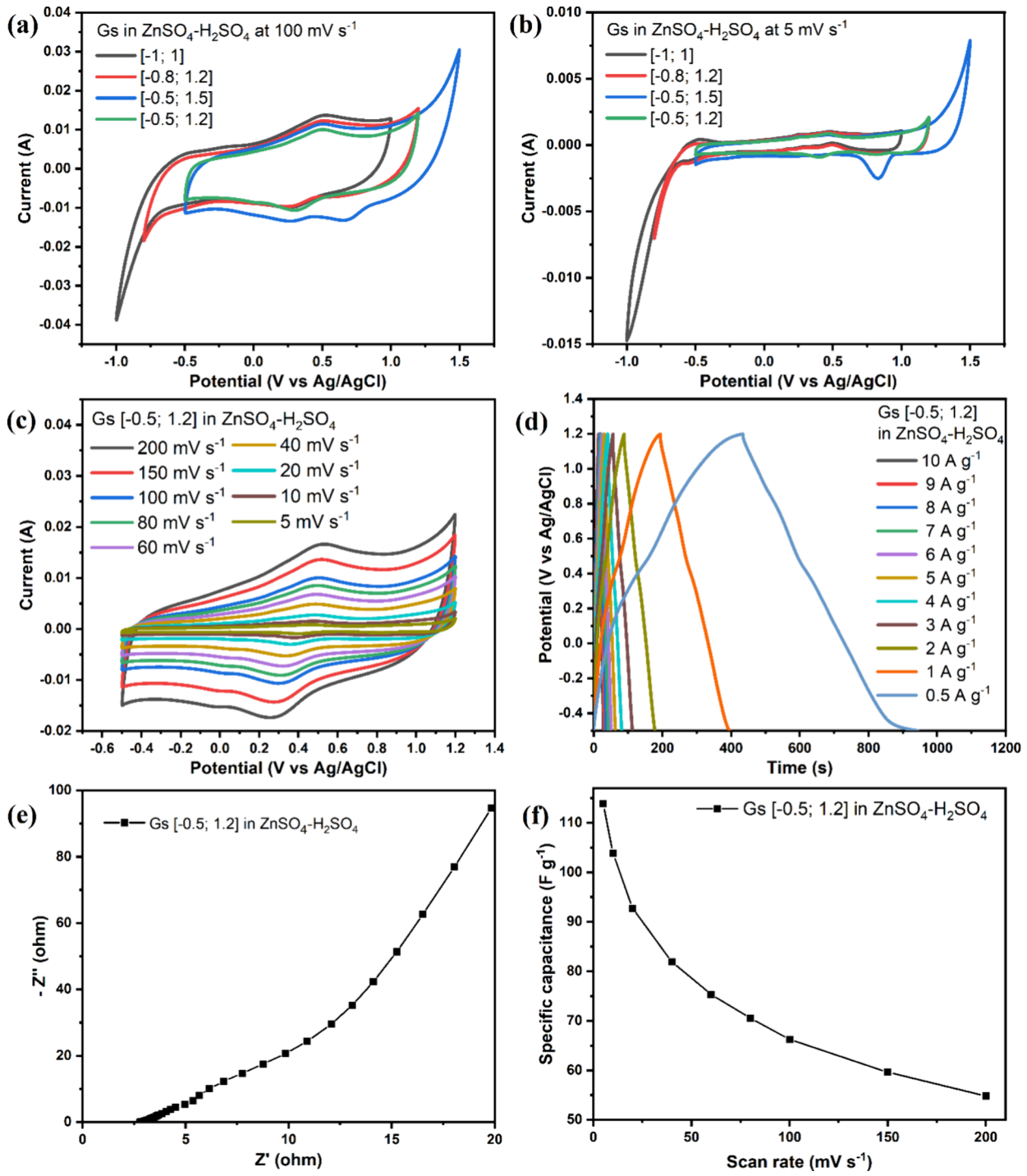

Figure 6. Electrochemical studies of the three-electrode system for Gs: CV curves at different working voltage windows (a) at 100 and (b) 5 mV s^{-1}, respectively, (c) CV curve in the range [−0.5; +1.2], (d) GCD curves in the range [−0.5; +1.2], (e) EIS plot, and (f) specific capacitances following scan rates.

profiles. The maximum energy density of the C_{NPs} working electrode is 39.59 W h kg^{-1} at a power density of 425 W kg^{-1}.

Figures 6 and 7 show the study of the electrochemical properties of Gs materials in a solution of $ZnSO_4$-H_2SO_4 electrolyte recycled from a spent zinc carbon battery. To investigate the electrochemical capability of the material in the redox additive in the aqueous electrolyte $ZnSO_4$-H_2SO_4, we carried out an electrochemical measurement survey of three electrodes via the CV curves at the measurement ranges of [−1; +1], [−0.8; +1.2], [−0.5; +1.5], and [−0.5; +12] (Figure 6a,b). At 100 mV s^{-1}, oxidation−reduction peaks in the [−1; +1], [−0.8; +1.2], and [−0.5; +1.5] regions can be clearly seen at 5 mV s^{-1}. Here, it can be seen that Gs material does not perform well in these regions, and it can also be seen that the material performs well in the [−0.5; +1.2] region. So, we selected the range [−0.5; +1.2] to further investigate the three-electrode electrochemical properties of Gs materials using CV, EIS, and GCD measurements. Figure 6c depicts the CV curve of the Gs electrode at −0.5 to +1.2 V in $ZnSO_4$-H_2SO_4. Here, the CV curve diagram at different scanning rates from 5 to 100 mV s^{-1}

https://doi.org/10.1021/acsomega.4c03948
ACS Omega 2024, 9, 27710−27721

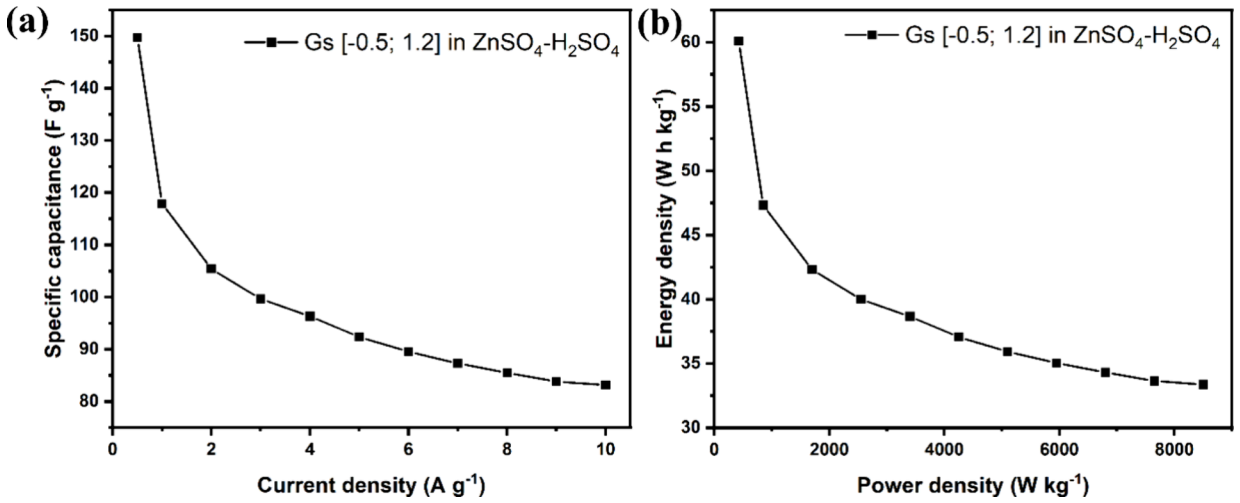

Figure 7. Electrochemical studies of the three-electrode system for Gs: (a) specific capacitances following current densities and (b) energy densities following power densities.

shows a rectangular CV curve with our redox peaks, showing the excellent capacitive behavior of the electrochemical double layer mechanism of symmetric redox peaks.[29,30] The GCD curve of the electrode Gs in $ZnSO_4$-H_2SO_4 electrolyte has been depicted in Figure 6d with a scan density between 0.5 and 10 A g^{-1}. The GCD diagram shows electrochemical properties corresponding to the CV diagram in Figure 6c, asserting that the material performs well between −0.5 and +1.2 V. Here, the GCD curve shows approximately equal intake and discharge paths, describing the ionic conductivity of the electrolyte through the electrode Gs as relatively stable. However, the Gs material was strongly reduced in the electrolyte $ZnSO_4$-H_2SO_4 at a current density of 0.5 A g^{-1}, resulting in a reduction path in the GCD measurement range that was larger than the discharge path but not significant. It was demonstrated through the Coulombic efficiency of carbon nanoparticles, as shown in Figure S2, that this demonstrates the charge−discharge stability of the material in the electrolyte solution. To investigate the ion transport of the $ZnSO_4$-H_2SO_4 electrolyte through the Gs electrode, an EIS measurement was performed and is depicted in Figure 6e. The equivalent resistance of the Gs electrode has a value of 2.78 Ω in the measurement range from 100 mHz to 100 kHz with an amplitude of 5 mV. The linear lines in low-frequency EIS diagrams show the capacitive effect of ionic diffusion,[31] while the Warburg impedance arises at high frequencies due to ionic diffusion resistance in the electrode layer.[32] Figure 6f depicts the specific capacitance of the Gs material calculated according to the formula eq 1 based on the CV curve with an increasing scan rate from 5 to 200 mV s^{-1}. The highest specific capacitance of the Gs electrode has a value of 113.9 F g^{-1} at 5 mV s^{-1} and the lowest value at 200 mV s^{-1} has a value of 54.82 F g^{-1}. Thereby, it can be seen that the material has a relatively stable ion transmittance of the electrode with the electrolyte solution $ZnSO_4$-H_2SO_4.

In addition, we also investigated the specific capacitance of the Gs electrode via the GCD curve and calculated it based on eq 2, as shown in Figure 7a. The highest capacitance of the Gs electrode is a value of 149.68 F g^{-1} at a scan density of 0.5 A g^{-1}, which is better than some carbon-based materials synthesized by different methods and shown in Table 1. At a high current density of 10 A g^{-1}, the Gs electrode still gives a good specific capacitance of 83.13 F g^{-1}. From Ragone cells, the electrode works Gs with the electrolyte $ZnSO_4$-H_2SO_4 giving the highest energy density value of 60.08 W h kg^{-1} at a power density of 425 W kg^{-1} (Figure 7b). In summary, the electrochemical properties of the Gs working electrode in $ZnSO_4$-H_2SO_4 electrolyte solution have shown excellent chemical stability of graphene nanosheets, prepared by exfoliation in table salt solution.

3.2.2. Electrochemical Studies of Devices. Based on the electrochemical stability of the material through three-electrode measurements of carbon nanoparticles and graphene nanosheet materials, the symmetrical solid-state supercapacitors were studied with a sandwich structure: electrode/gel polymer electrolyte/electrode. In which the polymer gel is made by mixing PVA with a 1 M $ZnSO_4$-H_2SO_4 solution, a gel solution is obtained that is applied to solid-state supercapacitors.

The cyclic voltammetry (CV) configuration for supercapacitors with carbon nanoparticle electrodes, C_{NPs}, is depicted in Figure 8a. Here, the CV curve of the symmetrical SSCs surveyed ranges from −0.5 to +1.2 V with varying scanning rates (from 5 to 200 mV s^{-1}) showing a semirectangular shape. With a semirectangular shape with no linear slope in this configuration, it has been shown to involve ion transport in PVA-$ZnSO_4$-H_2SO_4 gel electrolyte.[22] The high ion transport of the electrolyte to the electrode can be attributed to the material having a relatively high porosity, resulting in ions in the electrolyte going in and out of the electrode that take up a lot of time in the deeper pores in the lattice. This is a factor that affects the specific capacitance of the material. To better understand the ion transport in PVA-$ZnSO_4$-H_2SO_4 with a symmetric electrode, we proceeded to measure the EIS of the nanoparticle carbon component, as shown in Figure 8b. The Nyquist diagram of supercapacitor devices over the frequency range from 100 kHz to 100 mHz at 5 mV amplitude has shown that an equivalent impedance current has been found to be 2.64 Ω, including the intrinsic resistance of the carbon nanoparticles, the contact resistance of the interface-electrolyte electrode, and the ionic resistance of the electrolyte. Furthermore, the straight line of EIS components has shown good capacitive behavior that limits diffusion.[40] Figure 8c shows the GCD curves of supercapacitor devices measured with different scanning densities (from 0.5 to 10 A g^{-1}) with the electrolyte being PVA-$ZnSO_4$-H_2SO_4 gel. The curves were almost identical to triangles with relatively equal intake, and both lines showed a stable discharge and good

https://doi.org/10.1021/acsomega.4c03948
ACS Omega 2024, 9, 27710−27721

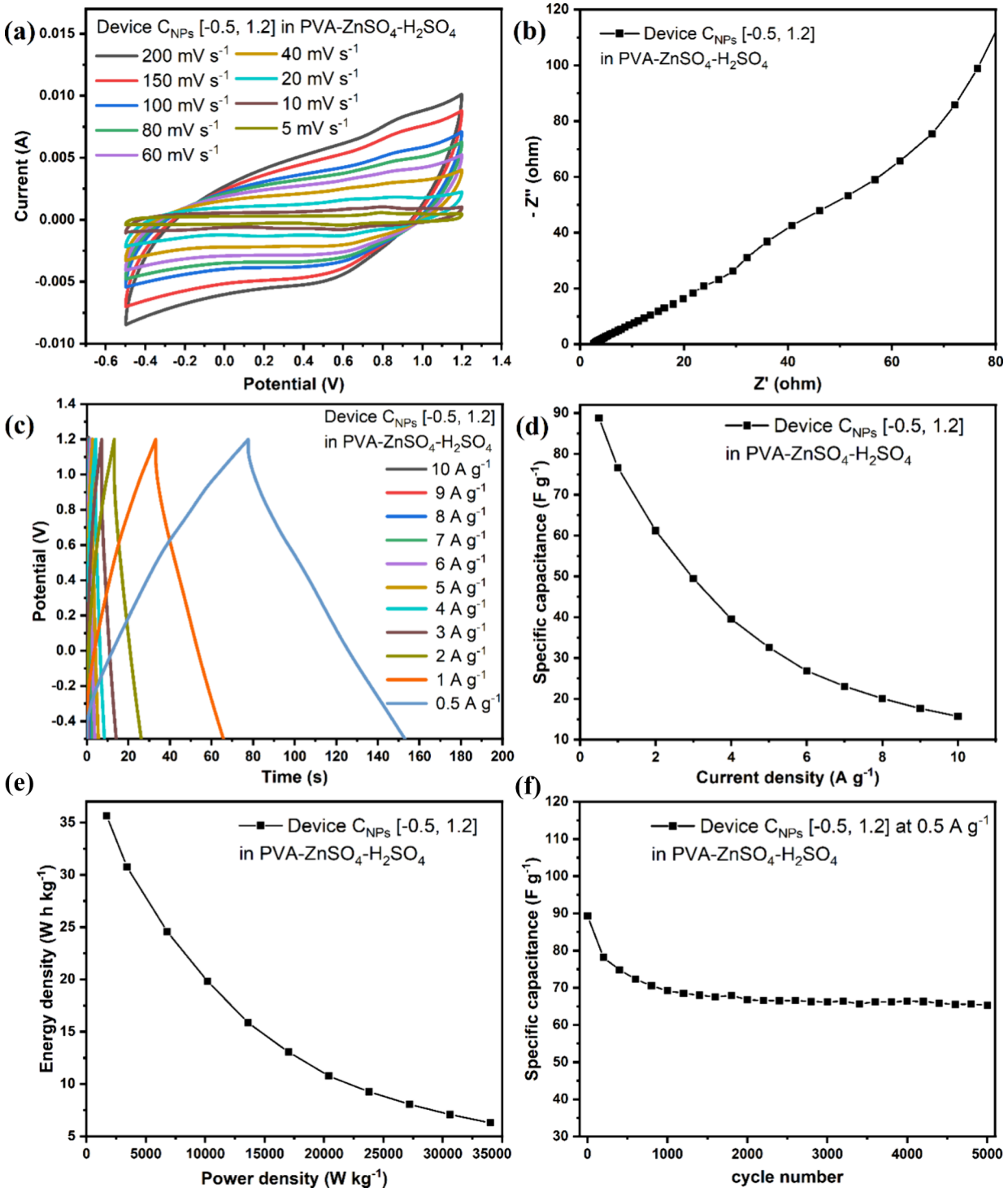

Figure 8. Electrochemical studies of devices C_{NPs}: (a) CV curves, (b) EIS plot, (c) GCD curves, (d,f) specific capacitance, and (e) energy densities following power densities.

electrochemical reversality. Based on the GCD diagram, the specific capacitance of the material has been calculated using eq 4 and plotted graphically in Figure 8d. The specific capacitance at different densities has shown that the symmetrical SSC devices using the PVA-$ZnSO_4$-H_2SO_4 gel as an electrolyte exhibits good electrochemistry with a value of 88.82 F g^{-1} at 0.5 A g^{-1}. Furthermore, the C_{NPs} symmetrical SSC devices exhibited a maximum energy density of 35.65 W h kg^{-1} at a power density of 1700 W kg^{-1} (Figure 8e). To investigate component strength, we measured cycle stability at 0.5 A g^{-1}. Over 5000 cycles, the specific capacitance of the material decreases to 73.1%, which indicates that the component has a relatively long service life. Thereby, it can be seen that the component works well in the PVA-$ZnSO_4$-H_2SO_4 gel electrolyte. Figure 8f shows the stability of symmetrical SSCs using C_{NPs} electrodes by charge-discharge over 5000 cycles at 0.5 A g^{-1}, which exhibits a good retention of 73.1%.

https://doi.org/10.1021/acsomega.4c03948
ACS Omega 2024, 9, 27710−27721

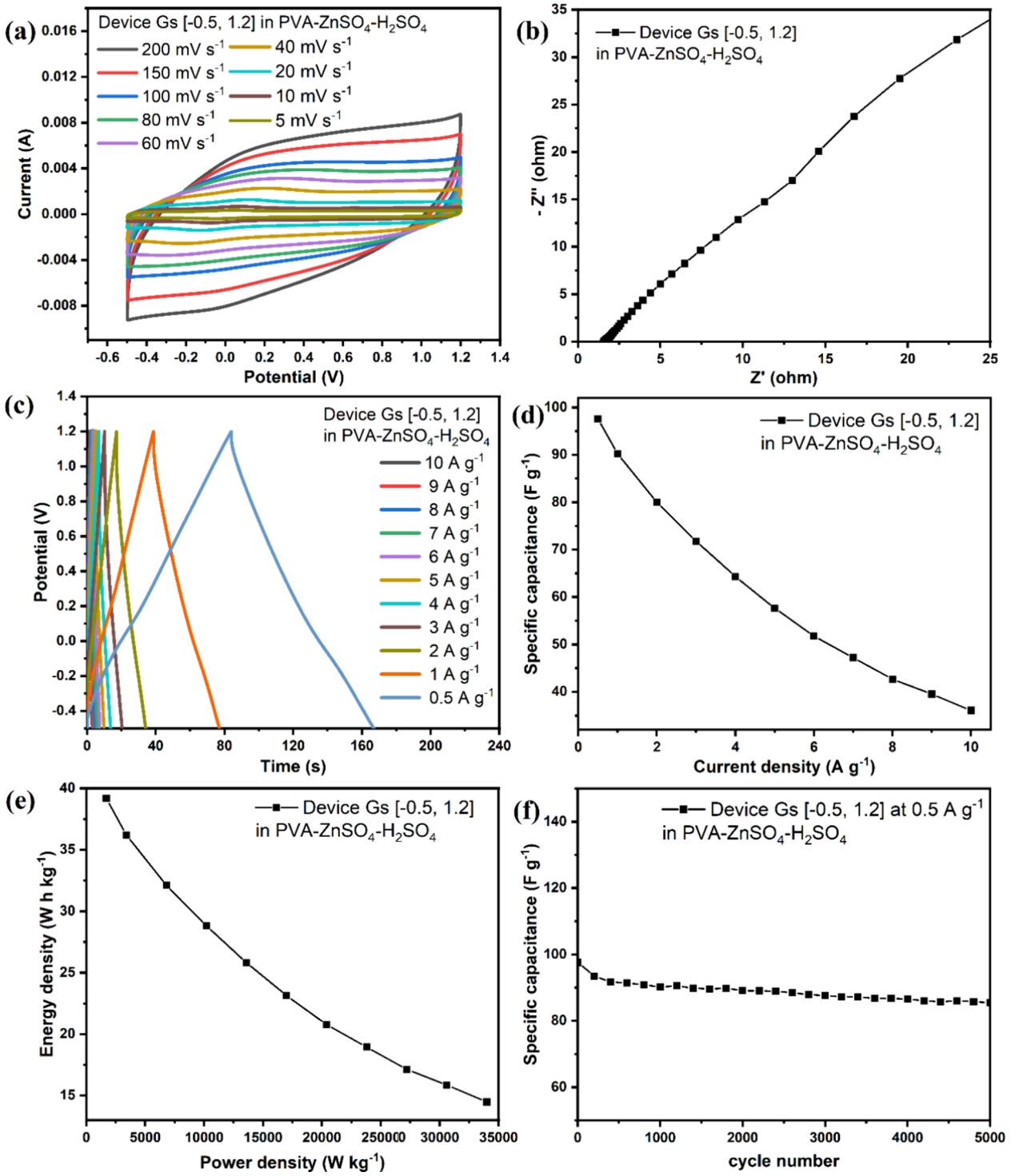

Figure 9. Electrochemical studies of devices Gs: (a) CV curves, (b) EIS plot, (c) GCD curves, (d,f) specific capacitance, and (e) energy densities following power densities.

Similar to carbon nanoparticles, the Gs components were also measured for electrochemical properties (CV, EIS, and GCD) with a PVA-$ZnSO_4$-H_2SO_4 gel polymer electrolyte in the active region from −0.5 to +1.2 V. Figure 9a depicts the CV curve schema surveyed with different measurement rates (from 5 to 200 mV s^{-1}) showing that the curve with a similar shape, equivalent to a rectangular shape, shows that the component has a relatively good capacitive behavior. The EIS diagram represents ion transport between the contact resistance of the interface-electrolyte electrode and the ionic resistance of the electrolyte (Figure 9b). Here, the impedance of the component with a value of 1.33 Ω indicates that the device has a low conductive resistance and an upward vertical line that leads to good capacitance and limits ionic diffusion. Figure 9c, depicting the GCD curves at different current densities (from 0.5 to 10 A g^{-1}) shows that the device is nearly linear and has a symmetric triangular shape, further showing its superior capacitance reversibility.[41] To study the electrochemical performance of

https://doi.org/10.1021/acsomega.4c03948
ACS Omega 2024, 9, 27710−27721

supercapacitor devices, the specific capacitance of supercapacitors at different current densities is calculated through GCD curves based on eqs 4 and 5, as shown in Figure 9d. The specific capacitance of a symmetrical device gives a maximum specific capacitance value of 97.6 F g^{-1} at 0.5 A g^{-1}. Figure 9e shows the relationship between the energy density and power density of cells in supercapacitors through Ragone diagrams that can be calculated from GCD configurations. The maximum power density of the Gs device is 39.17 W h kg^{-1} at a power density of 1700 W kg^{-1}. Furthermore, we conducted a material strength survey via GCD measurement at 0.5 A g^{-1} with 5000 cycles, as illustrated in Figure 9f. After 5000 cycles, the specific capacitance of the Gs symmetrical SSC device retained about 90.2% of its original capacitance. This proves that the material has a long service life, which makes it a good candidate for supercapacitors.

4. CONCLUSIONS

In summary, the new gel polymer electrolyte PVA-$ZnSO_4$-H_2SO_4 was successfully fabricated from zinc−carbon batteries. Additionally, carbon nanoparticles and graphene nanosheets were synthesized from carbon rods and carbon powder from used zinc−carbon batteries by an electrochemical exfoliation step in table salt and ultrasonic vibration. With a simple, easy, and low-cost recycling method to completely recycle zinc−carbon batteries, the supercapacitors exhibit relatively high capacitance and good stability. For supercapacitor applications, both graphene nanosheets and carbon nanoparticles have been shown to be stable over long periods of time, with Gs having a specific capacitance of 97.6 F g^{-1} at 0.5 A g^{-1} (∼90.2% retention) after 5000 cycles, while the C_{NPs} obtained a specific capacitance of 88.82 F g^{-1} after 5000 cycles (∼73.1% retention) and were relatively stable compared to the first cycle. These results provide a promising strategy for recycling electronic waste from zinc−carbon batteries, which are one of the most popular types of dry batteries.

■ ASSOCIATED CONTENT

Supporting Information

The Supporting Information is available free of charge at https://pubs.acs.org/doi/10.1021/acsomega.4c03948.

Process to synthesize $ZnSO_4$-H_2SO_4 redox additive electrolyte by dissolving zinc cans from spent zinc−carbon batteries in 1 M H_2SO_4 (MP4)

One symmetrical supercapacitor device can drive one small DC motor 0.5 V (MP4)

Figures showing the supercapacitor device and electrodes and Coulombic efficiency plots (PDF)

■ AUTHOR INFORMATION

Corresponding Authors

Nghia Trong Nguyen − *School of Chemical Engineering, Hanoi University of Science and Technology, Hanoi 100000, Vietnam*; Email: nghia.nguyentrong@hust.edu.vn

Thi Viet Bac Phung − *Center for Environmental Intelligence and College of Engineering and Computer Science, VinUniversity, Hanoi 100000, Vietnam*; orcid.org/0000-0001-7717-2538; Email: bac.ptv@vinuni.edu.vn

Authors

Thuy Trang T. Vuong − *Center for Environmental Intelligence and College of Engineering and Computer Science, VinUniversity, Hanoi 100000, Vietnam*

Huy-Trinh Phan − *Center for Environmental Intelligence and College of Engineering and Computer Science, VinUniversity, Hanoi 100000, Vietnam*; orcid.org/0009-0004-4337-8158

Nga Vu Thi Thu − *School of Chemical Engineering, Hanoi University of Science and Technology, Hanoi 100000, Vietnam*

Phi Long Nguyen − *Center for Environmental Intelligence and College of Engineering and Computer Science, VinUniversity, Hanoi 100000, Vietnam*

Huy Tiep Nguyen − *Faculty of Engineering Physics and Nanotechnology, VNU University of Engineering and Technology, Hanoi 100000, Vietnam*

Hoang V. Le − *Institute of Science and Technology, TNU-University of Sciences, Thai Nguyen 250000, Vietnam; University of Science and Technology of Hanoi, Vietnam Academy of Science and Technology, Hanoi 100000, Vietnam*

Phuoc-Anh Le − *Center for Environmental Intelligence and College of Engineering and Computer Science, VinUniversity, Hanoi 100000, Vietnam; Institute of Chemistry, Vietnam Academy of Science and Technology, Hanoi 100000, Vietnam*; orcid.org/0000-0003-4549-4166

Complete contact information is available at: https://pubs.acs.org/10.1021/acsomega.4c03948

Notes

The authors declare no competing financial interest.

■ ACKNOWLEDGMENTS

The authors acknowledge the support given by VinUniversity, Vietnam (VinUniversity Seed Grant, no. VUNI.2223.FT09).

■ REFERENCES

(1) Hassaan, M. A.; Nemr, A. E.; Madkour, F. F. Environmental assessment of heavy metal pollution and human health risk. *American Journal of Water Science and Engineering* **2016**, *2* (3), 14−19.

(2) Ukaogo, P. O.; Ewuzie, U.; Onwuka, C. V. Environmental pollution: causes, effects, and the remedies. *Microorganisms for sustainable environment and health*; Elsevier, 2020; pp 419−429; DOI: 10.1016/B978-0-12-819001-2.00021-8.

(3) Mrozik, W.; Rajaeifar, M. A.; Heidrich, O.; Christensen, P. Environmental impacts, pollution sources and pathways of spent lithium-ion batteries. *Energy Environ. Sci.* **2021**, *14* (12), 6099−6121.

(4) Yan, C.; Jin, M.; Pan, X.; Ma, L.; Ma, X. A flexible polyelectrolyte-based gel polymer electrolyte for high-performance all-solid-state supercapacitor application. *RSC Adv.* **2020**, *10* (16), 9299−9308.

(5) Cao, Z.; Hu, H.; Ho, D. Micro-Redoxcapacitor: A Hybrid Architecture Out of the Notorious Energy-Power Density Dilemma. *Adv. Funct. Mater.* **2022**, *32*, 2111805.

(6) Thanh, H. T. T.; Le, P. A.; Thi, M. D.; Le Quang, T.; Trinh, T. N. Effect of gel polymer electrolyte based on polyvinyl alcohol/polyethylene oxide blend and sodium salts on the performance of solid-state supercapacitor. *Bulletin of Materials Science* **2018**, *41*, 145.

(7) Gupta, A.; Jain, A.; Tripathi, S. K. Structural, electrical and electrochemical studies of ionic liquid-based polymer gel electrolyte using magnesium salt for supercapacitor application. *Journal of Polymer Research* **2021**, *28* (7), 235.

(8) Guo, H.; Ma, L.; Yan, C.; Ma, X. A study on the preparation of polycation gel polymer electrolyte for supercapacitors. *RSC Adv.* **2021**, *11* (40), 24995−25003.

(9) Chi, C.; Li, Y.; Li, D.; Huang, H.; Wang, Q.; Yang, Y.; Huang, B. Flexible solvent-free supercapacitors with high energy density enabled

by electrical-ionic hybrid polymer nanocomposites. *Journal of Materials Chemistry A* **2019**, *7* (28), 16748−16760.
(10) Yong, H.; Park, H.; Jung, C. Quasi-solid-state gel polymer electrolyte for a wide temperature range application of acetonitrile-based supercapacitors. *J. Power Sources* **2020**, *447*, 227390.
(11) Vuong, T.T. T.; Nguyen, P. L.; Nguyen, N. T.; Phung, T. V. B.; Le, P. A. Zinc-Carbon Battery Recycling for Investigating Carbon Materials for Supercapacitor Applications. *ACS Omega* **2024**, *9*, 22543.
(12) Le, P.-A.; Le, V. Q.; Nguyen, N. T.; Nguyen, V.-T.; Van Thanh, D.; Phung, T. V. B. Multifunctional applications for waste zinc−carbon battery to synthesize carbon dots and symmetrical solid-state supercapacitors. *RSC Adv.* **2022**, *12* (17), 10608−10618.
(13) Dawoud, H. D.; Al Tahtamouni, T.; Bensalah, N. Sputtered manganese oxide thin film on carbon nanotubes sheet as a flexible and binder-free electrode for supercapacitors. *International Journal of Energy Research* **2019**, *43* (3), 1245−1254.
(14) Sahu, V.; Shekhar, S.; Ahuja, P.; Gupta, G.; Singh, S. K.; Sharma, R. K.; Singh, G. Synthesis of hydrophilic carbon black; role of hydrophilicity in maintaining the hydration level and protonic conduction. *RSC Adv.* **2013**, *3* (12), 3917−3924.
(15) Wang, X.; Zhang, L. Green and facile production of high-quality graphene from graphite by the combination of hydroxyl radicals and electrical exfoliation in different electrolyte systems. *RSC Adv.* **2019**, *9* (7), 3693−3703.
(16) Bkrey, I. N.; Moniem, A. A. Flexible laser reduced graphene oxide/MnO2 electrode for supercapacitor applications. *Int. J. Chemical, Molecular, Nuclear, Materials and Metallurgical Eng.* **2014**, *8*, 951−957.
(17) Siburian, R.; Simanjuntak, C.; Supeno, M.; Lumbanraja, S.; Sihotang, H. New route to synthesize of graphene nano sheets. *Oriental journal of chemistry* **2018**, *34* (1), 182−187.
(18) Khamlich, S.; Abdullaeva, Z.; Kennedy, J. V.; Maaza, M. High performance symmetric supercapacitor based on zinc hydroxychloride nanosheets and 3D graphene-nickel foam composite. *Appl. Surf. Sci.* **2017**, *405*, 329−336.
(19) Li, J.; Liu, W.; Xiao, D.; Wang, X. Oxygen-rich hierarchical porous carbon made from pomelo peel fiber as electrode material for supercapacitor. *Appl. Surf. Sci.* **2017**, *416*, 918−924.
(20) Hamouda, H. A.; Cui, S.; Dai, X.; Xiao, L.; Xie, X.; Peng, H.; Ma, G. Synthesis of porous carbon material based on biomass derived from hibiscus sabdariffa fruits as active electrodes for high-performance symmetric supercapacitors. *RSC Adv.* **2021**, *11* (1), 354−363.
(21) Du, C. F.; Zhao, X.; Wang, Z.; Yu, H.; Ye, Q. Recent advanced on the MXene−organic hybrids: Design, synthesis, and their applications. *Nanomaterials* **2021**, *11* (1), 166.
(22) Ab. Rahim, A. H.; Ramli, N.; Nordin, A. N.; Abd. Wahab, M. F. Supercapacitor performance with activated carbon and graphene nanoplatelets composite electrodes, and insights from the equivalent circuit model. *Carbon Trends* **2021**, *5*, 100101.
(23) Yuan, G.; Liang, Y.; Hu, H.; Li, H.; Xiao, Y.; Dong, H.; Liu, Y.; Zheng, M. Extraordinary thickness-independent electrochemical energy storage enabled by cross-linked microporous carbon nanosheets. *ACS Appl. Mater. Interfaces* **2019**, *11* (30), 26946−26955.
(24) Zhao, G.; Li, Y.; Zhu, G.; Lu, T.; Pan, L. Biomass-based N, P, and S self-doped porous carbon for high-performance supercapacitors. *ACS Sustainable Chem. Eng.* **2019**, *7* (14), 12052−12060.
(25) Wu, D.; Cheng, J.; Wang, T.; Liu, P.; Yang, L.; Jia, D. A novel porous N-and S-self-doped carbon derived from chinese rice wine lees as high-performance electrode materials in a supercapacitor. *ACS Sustainable Chem. Eng.* **2019**, *7* (14), 12138−12147.
(26) Yang, S.; Wang, S.; Liu, X.; Li, L. Biomass derived interconnected hierarchical micro-meso-macro-porous carbon with ultrahigh capacitance for supercapacitors. *Carbon* **2019**, *147*, 540−549.
(27) Le, P. A.; Le, V. Q.; Nguyen, T. N.; Phung, T. V. B. Abundant agricultural biomass wastes-derived 3D porous carbon material for high performance supercapacitors. *Applied Nanoscience* **2023**, *13* (6), 3827−3838.
(28) Piwek, J.; Platek, A.; Fic, K.; Frackowiak, E. Carbon-based electrochemical capacitors with acetate aqueous electrolytes. *Electrochim. Acta* **2016**, *215*, 179−186.
(29) Cao, Z.; Liang, G.; Ho, D.; Zhi, C.; Hu, H. Interlayer Injection of Low-Valence Zn Atoms to Activate MXene-Based Micro-Redox Capacitors With Battery-Type Voltage Plateaus. *Adv. Funct. Mater.* **2023**, *33*, 2303060.
(30) Zhang, J.; Wang, K.; Lu, P.; Gao, J.; Cao, Z.; Mo, F.; Ho, D.; Li, B.; Hu, H. Wood-Like Low-Tortuosity Thick Electrode for Micro-Redoxcapacitor with Ultrahigh Areal Energy Density and Steady Power Output. *Adv. Funct. Mater.* **2024**, *34*, 2310775.
(31) Ahn, Y. K.; Kim, B.; Ko, J.; You, D. J.; Yin, Z.; Kim, H.; Kim, Y. S. All solid state flexible supercapacitors operating at 4 V with a cross-linked polymer−ionic liquid electrolyte. *Journal of Materials Chemistry A* **2016**, *4* (12), 4386−4391.
(32) Liu, D.; Li, Q.; Zhao, H. Electrolyte-assisted hydrothermal synthesis of holey graphene films for all-solid-state supercapacitors. *Journal of Materials Chemistry A* **2018**, *6* (24), 11471−11478.
(33) Xu, B.; Wu, F.; Su, Y.; Cao, G.; Chen, S.; Zhou, Z.; Yang, Y. Competitive effect of KOH activation on the electrochemical performances of carbon nanotubes for EDLC: Balance between porosity and conductivity. *Electrochim. Acta* **2008**, *53* (26), 7730−7735.
(34) Yong, S.; Owen, J.; Beeby, S. Solid-State Supercapacitor Fabricated in a Single Woven Textile Layer for E-Textiles Applications. *Adv. Eng. Mater.* **2018**, *20* (5), 1700860.
(35) Subramanian, V.; Luo, C.; Stephan, A. M.; Nahm, K. S.; Thomas, S.; Wei, B. Supercapacitors from activated carbon derived from banana fibers. *J. Phys. Chem. C* **2007**, *111* (20), 7527−7531.
(36) Yen, P. J.; Sahoo, S. K.; Chiang, Y. C.; Huang, S. Y.; Wu, C. W.; Hsu, Y. C.; Wei, K. H. Using different ions to tune graphene stack structures from sheet-to onion-like during plasma exfoliation, with supercapacitor applications. *Nanoscale Res. Lett.* **2019**, *14*, 1−11.
(37) AbdelHamid, A. A.; Elgamouz, A.; Kawde, A. N. Controlled electrochemical surface exfoliation of graphite pencil electrodes for high-performance supercapacitors. *RSC Adv.* **2023**, *13* (31), 21300−21312.
(38) Li, H. Y.; Yu, Y.; Liu, L.; Liu, L.; Wu, Y. One-step electrochemically expanded graphite foil for flexible all-solid supercapacitor with high rate performance. *Electrochim. Acta* **2017**, *228*, 553−561.
(39) Le, P. A.; Le, V. Q.; Nguyen, N. T.; Phung, V. B. T. Food seasoning-derived gel polymer electrolyte and pulse-plasma exfoliated graphene nanosheet electrodes for symmetrical solid-state supercapacitors. *RSC Adv.* **2022**, *12*, 1515−1526.
(40) Liu, Y.; Yan, D.; Zhuo, R.; Li, S.; Wu, Z.; Wang, J.; Geng, Z. Design, hydrothermal synthesis and electrochemical properties of porous birnessite-type manganese dioxide nanosheets on graphene as a hybrid material for supercapacitors. *J. Power Sources* **2013**, *242*, 78−85.
(41) Ma, Y.; Chen, D.; Fang, Z.; Zheng, Y.; Li, W.; Xu, S.; Yang, W. High energy density and extremely stable supercapacitors based on carbon aerogels with 100% capacitance retention up to 65,000 cycles. *Proc. Natl. Acad. Sci. U. S. A.* **2021**, *118* (21), No. e2105610118.

https://doi.org/10.1021/acsomega.4c03948
ACS Omega 2024, 9, 27710−27721